Light scattering by microscopic spheres behind a glass–air interface

Michael J. Jory

Thin Film Photonics Group, School of Physics, University of Exeter, Stocker Road, Exeter EX4 4QL, UK

Elaine A. Perkins

Detection, Defence Science and Technology Laboratory, Porton Down, Salisbury, Wiltshire SP4 0JQ, UK

J. Roy Sambles

Thin Film Photonics Group, School of Physics, University of Exeter, Stocker Road, Exeter EX4 4QL, UK

Received December 19, 2002; revised manuscript received March 10, 2003; accepted March 13, 2003

Scattering of light from single spheres placed behind a glass–air interface with light incident through the glass is examined. This scattering is investigated for both *p*- and *s*-polarized light incident at angles below the glass–air critical angle. The intensity of light scattered into the air half-space from each sphere is measured as a function of scattering angle, and this response is compared *in situ* with the background scatter produced by the planar substrate. A detailed comparison between data and established theory are thereby obtained. This system is of interest in the field of optical biosensing. © 2003 Optical Society of America

OCIS codes: 240.6700, 290.4020, 290.5820, 290.5850.

1. INTRODUCTION

The pioneering work describing the scattering of a plane, monochromatic wave by a homogeneous sphere of any diameter and composition was produced by Mie.[1] Subsequently, this theory has been extended by many authors to describe a wide range of systems. These include the spectral response of metallic suspensions, the study of atmospheric dust, the theory of the rainbow, and the effects of clouds and fog.[2,3]

More recently, there has been interest in how light scatters from a sphere placed on, near, or behind a planar surface.[4–15] In particular, Videen[15] has developed theory to model the way light scatters from a spherical air bubble in a glass substrate. Here, we test this same theory by comparison with experiment with respect to the scattering response of a sphere surrounded by a lower-index medium and illuminated through a material of high refractive index.

Such a system has many potential applications, especially when the phenomenon of evanescent light scattering is exploited. These include the total-internal-reflection microscope,[16–18] evanescent-wave-light-scattering measurements,[19–24] the characterization of thin absorbing films,[25,26] and optical sensing.[27–31] A more detailed discussion is provided in Ref. 32.

To evaluate the device potential of a particle–planar-surface system, it is essential to be able to predict the scattered intensity as a function of scattering angle (where scattering angle is measured from a normal to the planar surface in the transmitting half-space). A preliminary study has previously been conducted with a microscopic sphere placed behind a glass–air interface.[32] The data were acquired for a *p*-polarized incident beam and then compared to the theory described in Ref. 15. Good agreement was found between the general shape of the experimentally measured intensity profiles and those predicted by theory, but little correlation in the mode structure was evident.

We extend the work reported in Ref. 32 by studying the scattering response for both *p*- and *s*-polarizations, minimizing the effects of surface roughness and surface contamination of the glass substrate, and investigating the response of two different size spheres (5-μm and 1.4-μm diameters). A new experimental configuration is also used which allows direct comparison between the scattering response of the sphere behind the glass–air interface and that of the interface alone. As in Ref. 32, the experimental scattering profiles are compared to those predicted by Videen theory.[15] (All the data presented here are for angles of incidence below the glass–air critical angle).

2. EXPERIMENTAL

Isopropyl alcohol (IPA) and an appropriate quantity of glass microspheres (5-μm diameter, 1.52 refractive index) are used to form a particulate suspension ($\sim$0.001 kg/m^3). A 20-μl drop of this suspension is placed on the surface of a fusion-drawn glass slide of refractive index 1.52. [Corning 7509 fusion-drawn glass is chosen as it has a very low surface roughness ($\sim$13 nm)[33]]. Once the IPA has evaporated, the microsphere-covered surface is examined under a high-power microscope (400×). Individual spheres are readily observed. The surface is examined until a single, isolated sphere is found, i.e., a sphere that is separated from all other spheres, any dust particles,

and any blemishes in the surface of the glass substrate by at least 100 μm. A series of photographs is now taken to provide a map of the surface to be used later to relocate the chosen isolated particle.

This glass slide is placed on the hypotenuse face of a 45°, 45°, 90° glass prism (refractive index 1.52); a drop of oil (also of index 1.52) is used to form a refractive-index-matching layer [Fig. 1(a)]. The top corner of the slide is then attached to a translation stage that has previously been mounted on the prism face to allow the horizontal position of the sample to be adjusted. The flat face of a cylindrical lens is bonded to a glass block by a UV-cured glue[34] and this assembly is placed on one of the remaining faces of the prism, again with the index-matching oil. The thickness of the glass block is chosen such that the distance from the outer (i.e., sphere-covered) surface of the glass slide to the curved surface of the cylindrical lens is approximately equal to the radius of curvature of the latter [Fig. 1(a)]. This distance may now be precisely adjusted—so as to account for the thickness of the glass slide—by sliding the lens–block assembly along the prism face. Thus, an optical beam passing through the cylindrical lens at a normal to the curved surface will always strike the same point of the glass slide regardless of incident angle.

The entire prism assembly is now positioned so that the sphere-populated surface of the glass slide is at the center of a rotatable table [Fig. 1(b)]. The 2-mm wide, 10-mW, polarized beam (of wavelength 632.8 nm) from a helium-neon laser is then directed through the cylindrical lens (which focuses the beam in the horizontal plane) and the prism onto the outer, sphere-covered, surface of the glass slide. (A second cylindrical lens of focal length 15 cm is placed before the prism assembly to focus the beam in the vertical plane). It is now possible to rotate the table to select an angle of incidence while ensuring that the position at which the optical beam strikes the surface of the glass slide remains fixed.

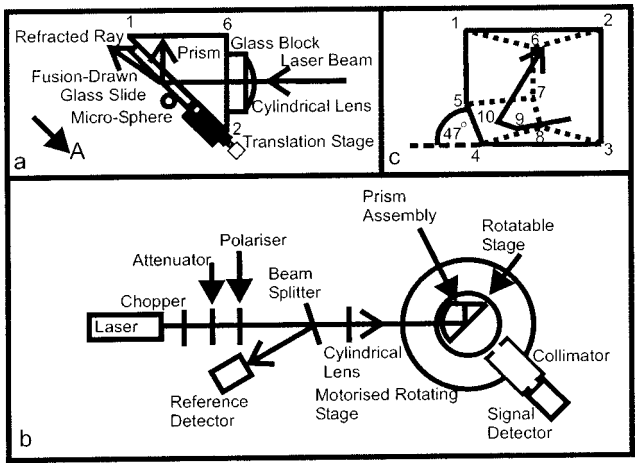

Fig. 1. (a) Prism assembly. The distance from the curved surface of the cylindrical lens to the outer surface of the glass slide is equal to the radius of curvature of the former. When the sample is positioned so as to measure the scattering response of the glass slide alone, the laser beam strikes the surface of the glass slide so that the refracted ray does not strike the sphere. (b) Experimental arrangement. (c) The modified prism. (The hypotenuse face 1,2,3,4,5 is foremost). The bottom of the exit face of the prism is machined at an angle of 47° to produce face 4,5,7,8. After partial reflection at the sample surface (9) the laser beam strikes face 4,5,7,8. Consequently, any light reflected here as the beam leaves the prism is directed away from the surface of the glass slide. (For clarity, only the prism itself is shown here).

The remaining face of the prism has previously been machined and polished at an angle of 47° to prevent any light reflected here from striking the interface under investigation [see Fig. 1(c)]. All optical elements in this system, including the prism, glass slide and lenses, are cleaned with cotton buds soaked in IPA. Further cleaning is accomplished by dragging an IPA-soaked lens tissue across the faces of each element.

An angle of incidence is now selected using the rotatable table. The microspheres are then viewed (*in situ*) through a retractable-arm-mounted microscope[35]; with the photographic map of the surface, the previously chosen isolated sphere is now located. The translation stage attached to the glass slide allows the horizontal position of the sample to be adjusted (without perturbing the rest of the optics) so that the isolated microsphere is positioned centrally within the laser beam spot (approximately 50-μm radius). At this stage, the surface is again examined through the microscope to ensure that the only scattered light observable is from the microsphere, and that no dust particles have contaminated the sample. The translation stage is now readjusted so as to move the sphere out of the beam. To avoid the refracted ray accidentally impinging on the sphere, the sample is moved in the direction of arrow A [Fig. 1(a)]. The surface is again checked to ensure that there are no dust particles in the beam spot. Having aligned the system in the "no-particle" position, the microscope is moved away from the prism.

A photomultiplier tube detector is placed on a second, motorized, rotating table whose rotation axis coincides with that of the first. Scattered intensity is now recorded while the scattering angle is incremented from −90° to +90°. The angle over which the scattered light is collected is controlled by two apertures (each of diameter 1 mm) placed between the prism and the detector that act as collimators. For these experiments the collection angle is set to 0.8°. Data are acquired for both *p*- and *s*-polarized input beams. While the observer views the sample surface with the microscope, the isolated microsphere is now moved back into the center of the laser beam spot with the translation stage. Total scattered intensity as a function of scattering angle is again recorded for both input polarizations. The above process is repeated for internal angles of incidence of 31°, 34°, and 37° (all below the glass–air critical angle).

Similar measurements are taken for a single latex sphere (refractive index 1.60) of approximate diameter 1.4 μm. As the total intensity of light scattered from this sphere is less than that from the 5-μm sphere, it is essential to reduce the beam spot size to obtain sufficient contrast between the signal from the sphere and that from the substrate. Consequently, the laser beam is now expanded from its initial 2-mm width to 1 cm and the second cylindrical lens is replaced with a spherical lens of focal length 10 cm. By viewing the sample surface with the *in situ* microscope, the sphere is then positioned in the center of the laser beam spot using the method de-

scribed above. The combined focusing of the spherical lens and the cylindrical lens (attached to the prism) produces an elliptical beam spot. The height of the beam spot is further reduced using an adjustable slit aperture until it is approximately 10 μm in diameter.

3. THEORY

To model the way light scatters from a single microscopic sphere placed behind a planar interface, it is necessary to address how radiation may interact with the system. For angles of incidence below the critical angle, the incident plane wave strikes the particle after refraction at the planar interface.

Now, the far-field radiation in the half-space containing the sphere is the result of a superposition of fields scattered directly from the sphere and those from the sphere that are then reflected from the planar interface. (It is assumed that the scattered fields from the sphere that reflect off the planar interface and interact with the sphere again are much weaker than the incident plane wave). Both effects are accounted for by including the appropriate transmission and reflection coefficients for the planar interface in the theory. These coefficients are calculated from Fresnel equations.[36] In combining Mie theory with Fresnel theory in this way, it is possible to describe the scattering response of the system by defining a 2×2 amplitude-scattering matrix S where E_{inc} and E_{sca} are the incident and scattered fields, respectively, $E_{\mathrm{sca}} \propto SE_{\mathrm{inc}}$, and $S = \begin{bmatrix} S_2 & S_3 \\ S_4 & S_1 \end{bmatrix}$. For in-plane scattering, only the leading diagonal elements of this matrix are nonzero. The equations required to evaluate S_1 (s-polarized light) and S_2 (p-polarized light) are given in Ref. 15.

4. RESULTS

Figure 2 compares experimental data and predicted theory for the 5 μm sphere when illuminated at an incident angle of 31°. The light solid curve (referred to the left-hand axis) indicates the scattering response from the sphere, while the heavy solid curve shows the intensity profile obtained when the sphere is moved out of the laser beam spot. (In the latter case, the laser beam strikes an area of the fusion-drawn glass slide surface that is unoccupied by a sphere). Thus, a direct comparison is obtained between the scattering response of the sphere and the effects of light scattering from the surface roughness associated with the substrate. In both cases, there is a large peak in intensity corresponding to the refracted beam at a scattering angle of 51°. When the laser beam spot is centered on the sphere, the detected signal here is the sum of light scattered from the sphere (in a direction coincident with the angle of the refracted beam) and that part of the beam which is simply refracted at the glass–air interface without having interacted with the sphere. However, at scattering angles away from the refracted beam direction, the background signal is at least an order of magnitude lower than that obtained from the sphere. Thus, the clear mode structure observed can be due only to scattering from the sphere, and cannot have been caused by surface roughness scattering or by some other process, e.g., a stray beam that has undergone multiple reflections within the prism. When we theoretically model the scattering response of the system, the effects of adjusting both the radius and refractive index of the sphere are investigated for both p- and s-incident polarizations. The best agreement between data and theory (open circles referred to the right-hand axis) is achieved by using the given value 1.52($\pm$0.01) for the sphere refractive index and a value of 5.14($\pm$0.01) μm for the sphere diameter. Conventionally, light-scattering intensity profiles are plotted on a logarithmic scale (see, for example, Ref. 37) but in this work, to obtain a detailed comparison between experiment and theory, all data are plotted on a linear scale. Both the angular position and relative heights of many of the peaks correlate. Additionally, there are differences in mode structure observed in the experimental data for scattering angles between $-30°$ and 30° that are associated with switching between p- and s-polarized light. These differences are replicated in the theory curves. Figure 3 shows the same data on

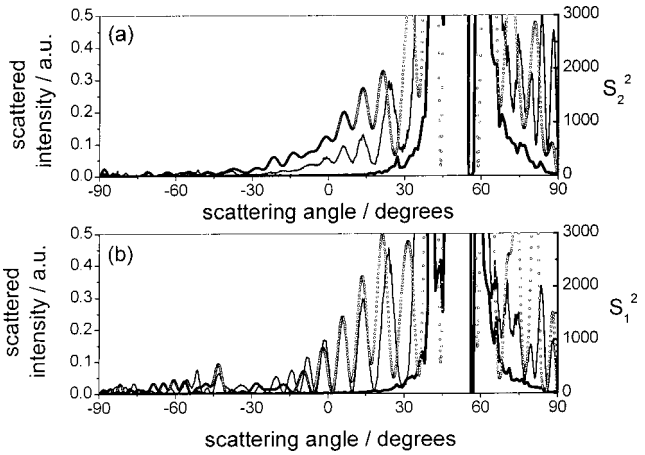

Fig. 2. Total scattered intensity versus scattering angle (light scattering profile) for a 5-μm diameter glass sphere placed behind a glass–air interface and illuminated with light at an angle of incidence of 31.0° (below the critical angle). The light solid curves and dotted curves are the experimental data (left-hand axis) and predicted theory (right-hand axis), respectively. The heavy solid curve (left-hand axis) indicates the experimentally measured response of the planar glass surface alone (i.e., no sphere). (a) p-polarized incident beam, (b) s-polarized incident beam.

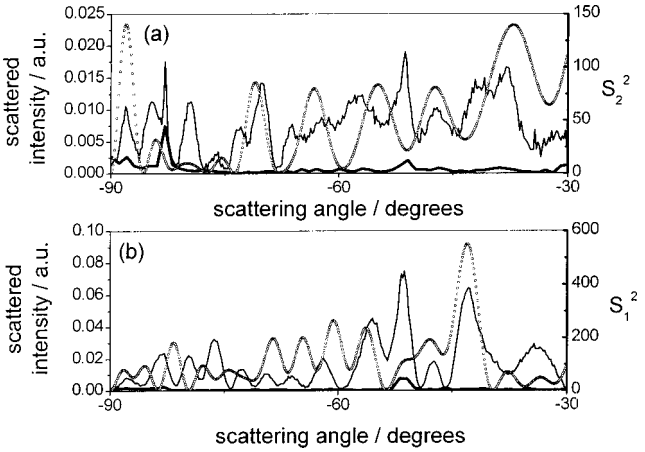

Fig. 3. Data from Fig. 2 shown on an expanded scale for scattering angles between $-90°$ and $-30°$.

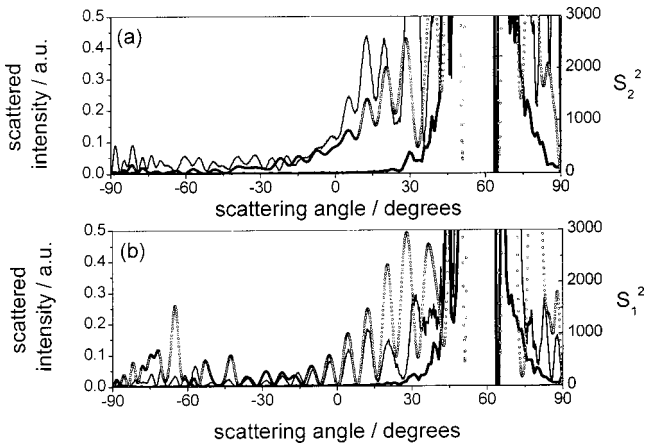

Fig. 4. Light-scattering profile for the same system as in Fig. 2, but illuminated at an angle of incidence of 34.0°. (a) *p*-polarized incident beam, (b) *s*-polarized incident beam. The experimentally measured scattering responses from the sphere and substrate are indicated by the light solid and heavy solid curves, respectively, and compared with the response predicted by theory (dotted curves).

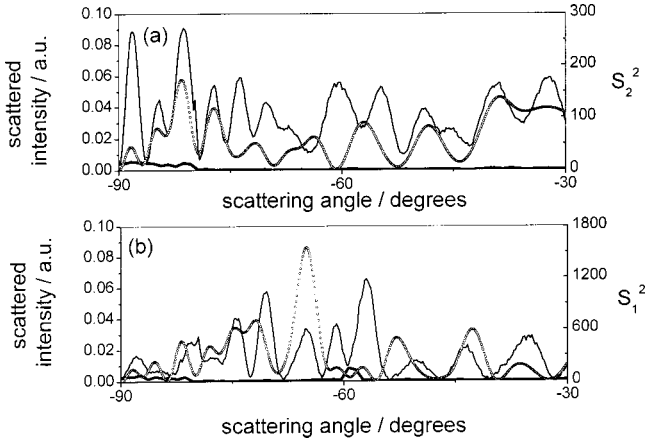

Fig. 5. Data from Fig. 4 shown on an expanded scale for scattering angles between −90° and −30°.

an expanded scale for scattering angles between −90° and −30°. On this expanded scale, it is clear that there are major discrepancies between data and theory over this angle range, with few of the peaks in intensity correlating in terms of angular position and relative strength for scattering angles beyond −60°.

Figures 4 and 5, and Fig. 6, compare data and theory for angles of incidence equal to 34.0° and 37.0°, respectively. Again, there is little correlation between the experimentally measured scattering response and that predicted by theory for scattering angles beyond −60°. However, both the angular position and relative heights of many of the intensity peaks correlate for scattering angles between −60° and 90°. The differences in mode structure observed in the experimental data for scattering angles between −30° and 30° that are associated with switching between *p*- and *s*-polarized light are also replicated in the theory curves.

Figures 7 and 8 show the data acquired from a 1.4-μm diameter latex bead (refractive index 1.60). Again, the light solid curves represent the signal obtained from the sphere and the heavy solid curves, the signal recorded from the substrate alone. In both figures there is a clear mode structure associated with scattering from the sphere that is not present in the background signal. However, as there is less scattered intensity from this smaller sphere, the contrast between sphere and background signal is not as good as for the data acquired from the 5-μm sphere. The background signal is therefore subtracted from the scattering response acquired for the sphere [Figs. 9 and 10 (solid curves)]. (Subtraction of one data set from the other produces a very noisy response at scattering angles in the region of the refracted ray, so in both cases, for the sake of clarity, these data points are not shown.)

The open circles (Figs. 9 and 10) indicate the response predicted by theory. Again, the effects of adjusting both

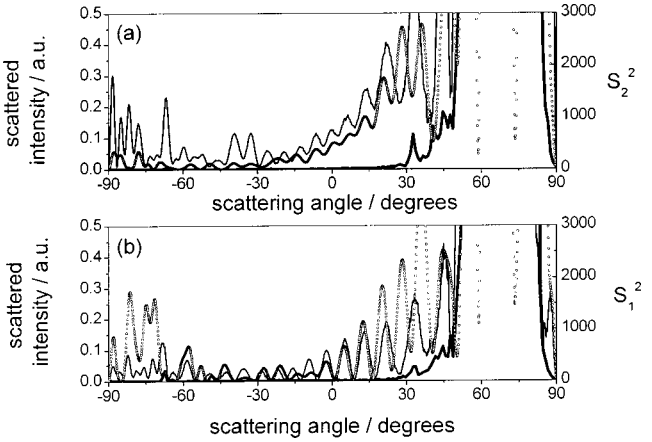

Fig. 6. Light-scattering profile for the same system as Fig. 2 but illuminated at an angle of incidence of 37.0°. (a) *p*-polarized incident beam, (b) *s*-polarized incident beam. The experimentally measured scattering responses from the sphere and substrate are indicated by the light solid and heavy solid curves, respectively, and compared to the response predicted by theory (dotted curves).

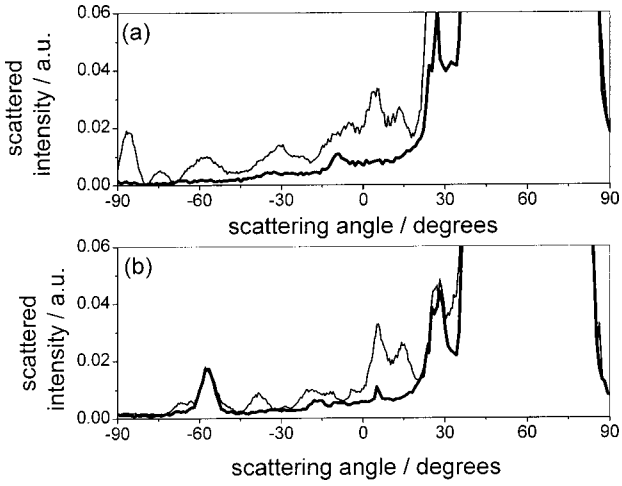

Fig. 7. Total scattered intensity versus scattering angle (light scattering profile) for a 1.5-μm diameter latex sphere placed behind a glass–air interface and illuminated with light at an angle of incidence of 35.0°. The light solid and heavy solid curves are the experimental data acquired for the sphere and the substrate, respectively. (a) *p*-polarized incident beam, (b) *s*-polarized incident beam.

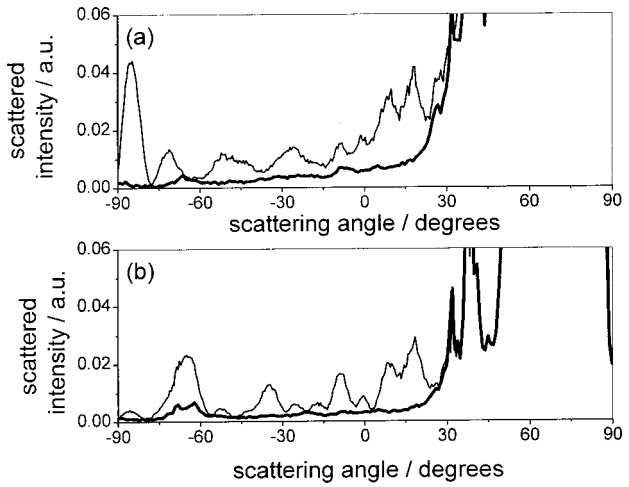

Fig. 8. Same as in Fig. 7 but angle of incidence is 37.0°.

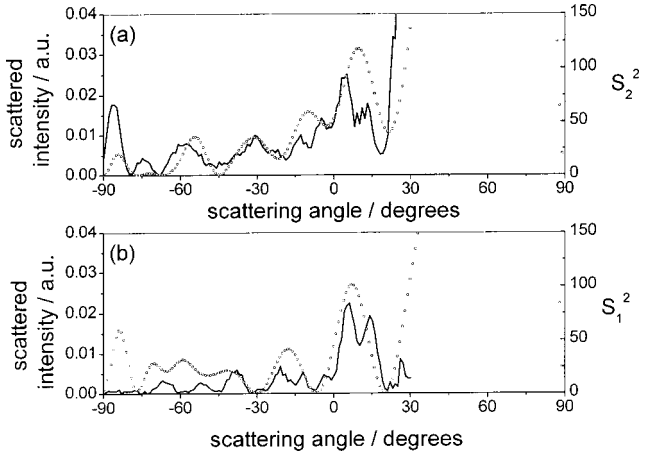

Fig. 9. Experimental data, light-scattering profile, for the same sphere and angle of incidence as for Fig. 7, having subtracted the background signal (solid curve, left-hand axis). The dotted curves show the corresponding response predicted by theory (right-hand axis).

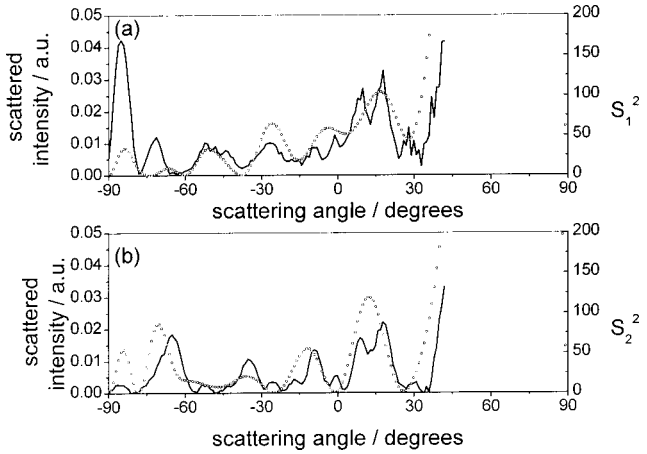

Fig. 10. Experimental data, light-scattering profile, for the same sphere and angle of incidence as for Fig. 8, having subtracted the background signal (solid curve, left-hand axis). The dotted curves show the corresponding response predicted by theory (right-hand axis).

the radius and refractive index of the sphere are investigated for both *p*- and *s*-incident polarizations. The best agreement between data and theory is achieved with the given value of 1.6(±0.01) for the sphere refractive index and a value of 1.50(±0.01) μm for the sphere diameter. There is reasonable agreement between data and theory, with the positions and relative intensities of several of the peaks correlating.

It should be noted that the fine structure evident in all the experimentally obtained curves is not random noise but is, in fact, a highly repeatable characteristic of the scattering system. Further investigation is required to explain this, but it may be due to scattering from the surface roughness associated with the glass substrate coupling with the scattering from the sphere, or perhaps scattering from the surface roughness of the sphere itself.

5. CONCLUSIONS

The angle-dependent scattering response of a single microscopic sphere placed behind a glass–air interface was studied for both *p*- and *s*-incident polarizations. Single spheres of diameters 5 μm and 1.4 μm (with refractive indices 1.52 and 1.60, respectively) were used. Care was taken to minimize the effects of light scattering from surface roughness associated with the glass substrate and surface contaminants. In all cases, the scattering response of the sphere behind the glass–air interface was compared with that of the interface alone. Thus, detailed comparison and reasonable agreement are obtained between the experimentally measured scattering response of the system and that predicted by theory.

The remaining discrepancies between data and theory may be due to the scattered fields's from the sphere that reflect off the planar interface and interact again with the sphere not being included in the model. Alternatively, these differences might be due to a slight ellipticity of the sphere. Even better agreement may be obtained by applying a theory that would account for the latter (see, for example, Refs. 38–40), or by using a much larger sphere (~20-mm diameter) and studying the system using microwave radiation (of wavelength ~5 mm). The latter may allow the shape of the particle and its surface roughness, along with the surface roughness of the substrate, to be controlled precisely.

Having compared in detail the experimentally measured scattering response with that predicted by theory for light incident below the glass–air critical angle, the work will now be extended to encompass higher angles of incidence. This will allow the enhanced light scattering from particles placed in the evanescent fields associated with total internal reflection[16–18] and surface-plasmon resonance[41–43] to be studied. As the spheres used are similar to biological particles in both size and refractive index, this may have important ramifications in the field of optical biosensing.[43]

ACKNOWLEDGMENTS

M.J. Jory gratefully acknowledges funding for a research fellowship under the Joint Grant Scheme from the Defence Science and Technology Laboratory, Porton Down,

and the Engineering and Physical Sciences Research Council (UK). The authors also acknowledge the technical help of P. S. Cann.

Corresponding author M.J. Jory may be reached by e-mail at mjjory@exeter.ac.uk.

REFERENCES AND NOTES

1. G. Mie, "Beitrage zur optik truber medien speziell kolloidaler metallosungen," Ann. Phys. **25**, 377–445 (1908).
2. M. Born and E. Wolf, *Principles of Optics* (Pergamon, New York, 1980).
3. H. C. Van De Hulst, *Light Scattering by Small Particles* (Dover, New York, 1981).
4. P. A. Bobbert and J. Vlieger, "Light-scattering by a sphere on a substrate," Physica A **137**, 209–242 (1986).
5. I. V. Lindell, A. H. Sihvola, K. O. Muinonen, and P. W. Barber, "Scattering by a small object close to an interface. I. Exact-image theory formulation," J. Opt. Soc. Am. A **8**, 472–476 (1991).
6. K. O. Muinonen, A. H. Sihvola, I. V. Lindell, and K. A. Lumme, "Scattering by a small object close to an interface. 2. Study of backscattering," J. Opt. Soc. Am. A **8**, 477–482 (1991).
7. G. Videen, "Light-scattering from a sphere on or near a surface," J. Opt. Soc. Am. A **8**, 483–489 (1991); errata, **9**, 844–845 (1992).
8. A. Doicu, Y. A. Eremin, and T. Wriedt, "Convergence of the T-matrix method for light scattering from a particle on or near a surface," Opt. Commun. **159**, 266–267 (1999).
9. T. Wriedt and A. Doicu, "Light scattering from a particle on or near a surface," Opt. Commun. **152**, 376–384 (1998).
10. A. Doicu, Y. Eremin, and T. Wriedt, "Non-axisymmetric models for light scattering from a particle on or near a plane surface," Opt. Commun. **182**, 281–288 (2000).
11. C. Liu, T. Weigel, and G. Schweiger, "Structural resonances in a dielectric sphere on a dielectric surface illuminated by an evanescent wave," Opt. Commun. **185**, 249–261 (2000).
12. R. Wannemacher, A. Pack, and M. Quinten, "Resonant absorption and scattering in evanescent fields," Appl. Phys. B Lasers Opt. **68**, 225–232 (1999).
13. B. J. Soller and D. G. Hall, "Dynamics modifications to the plasmon resonance of a metallic nanoparticle coupled to a planar waveguide: beyond the point-dipole limit," J. Opt. Soc. Am. B **19**, 1195–1203 (2002).
14. H. Ishikawa, H. Tamaru, and K. Miyano, "Microsphere resonators strongly coupled to a plane dielectric substrate: coupling via the optical near field," J. Opt. Soc. Am. A **17**, 802–813 (2000).
15. G. Videen, "Light-scattering from a sphere behind a surface," J. Opt. Soc. Am. A **10**, 110–117 (1993).
16. D. C. Prieve, F. Lanni and F. Luo, "Brownian-motion of a hydrosol particle in a colloidal force-field," Faraday Discuss. **83**, 297–307 (1987).
17. D. C. Prieve and N. A. Frej, "Total internal-reflection microscopy—a quantitative tool for the measurement of colloidal forces," Langmuir **6**, 396–403 (1990).
18. M. A. Brown, A. L. Smith and E. J. Staples, "A method using total internal-reflection microscopy and radiation pressure to study weak interaction forces of particles near surfaces," Langmuir **5**, 1319–1324 (1989).
19. I. Braslavsky, R. Amit, B. M. J. Ali, O. Gileadi, A. Oppenheim, and J. Stavans, "Objective-type dark-field illumination for scattering from microbeads," Appl. Opt. **40**, 5650–5657 (2001).
20. G. A. Schumacher and T. G. M. Vandeven, "Evanescent wave scattering studies on latex–glass interactions," Langmuir **7**, 2028–2033 (1991).
21. Z. M. Xia and T. G. M. Vandeven, "Adhesion kinetics of phosphatidylcholine liposomes by evanescent wave light-scattering," Langmuir **8**, 2938–2946 (1992).
22. M. Polverari and T. G. M. Vandeven, "Electrostatic and steric interactions in particle deposition studied by evanescent-wave light-scattering," J. Colloid Interface Sci. **173**, 343–353 (1995).
23. W. J. Albery, G. R. Kneebone, and A. W. Foulds, "Kinetics of colloidal deposition studied by a wall-jet cell," J. Colloid Interface Sci. **108**, 193–198 (1985).
24. W. J. Albery, R. A. Fredlein, G. R. Kneebone, G. J. O'Shea, and A. L. Smith, "The kinetics of colloidal deposition under conditions of controlled potential," Colloids Surf. **44**, 337–356 (1990).
25. F. Yang, J. R. Sambles, and G. W. Bradberry, "Determination of the optical constants and thickness of a highly absorbing film using the attenuated total reflection technique," J. Mod. Opt. **38**, 1441–1450 (1991).
26. S. C. Kitson and J. R. Sambles, "Critical edge studies of highly absorbing anisotropic films," Thin Solid Films **229**, 128–132 (1993).
27. B. Mizaikoff, "Mid infra-red evanescent wave sensors—a novel approach for subsea monitoring," Meas. Sci. Technol. **10**, 1185–1194 (1999).
28. C. Malins, M. Landl, P. Simon, and B. D. MacCraith, "Fiber optic ammonia sensing employing novel near infrared dyes," Sens. Actuators B **51**, 359–367 (1998).
29. L. T. Gao, C. J. Seliskar and L. Milstein, "Spectroscopic sensing with a highly transparent, ion-exchangeable polymer blend," Appl. Spectrosc. **51**, 1745–1752 (1997).
30. G. O'Keeffe, B. D. MacCraith, A. K. McEvoy, C. M. McDonagh, and J. F. McGilp, "Development of a LED-based phase fluorometric oxygen sensor using evanescent-wave excitation of a sol-gel immobilised dye," Sens. Actuators B **29**, 226–230 (1995).
31. S. McCabe and B. D. MacCraith, "Novel mid infra-red LED as a source for optical-fiber gas-sensing," Electron. Lett. **29**, 1719–1721 (1993).
32. M. J. Jory, S. N. Swatton, E. Perkins, N. J. Geddes, and J. R. Sambles, "Measurement of light scattering from a dielectric sphere behind a glass/air interface," J. Mod. Opt. **48**, 565–572 (2001).
33. Corning 7509 fusion-drawn glass supplied by Gooch and Housego Ltd., The Old Magistrates Court, Ilminster, Somerset, TA19 OAS, UK; http://www.goochandhousego.com.
34. UV-cured glue, Norland Optical Adhesive 65, refractive index 1.52, supplied by Tech Optics Ltd., Unit 6, Cala Industrial Estate, Tonbridge, Kent, UK; http://www.norlandprod.com.
35. *In situ* microscope, Intel Play microscope supplied by Intel Corporation UK Ltd, Pipers Way, Swindon, Wiltshire, SN3 1RJ, UK; http://www.intel.com.
36. E. Hecht, *Optics* (Addison-Wesley, London, 1987), p. 107.
37. G. Videen and D. Ngo, "Light scattering from a cylinder near a plane interface: theory and comparison with experiment," J. Opt. Soc. Am. A **14**, 70–78 (1997).
38. G. Videen, Q. Fu, and P. Chylek, "Special issue—light scattering by non-spherical particles-preface," J. Quant. Spectrosc. Radiat. Transf. **70**, 373–374 (2001).
39. G. Videen and D. Secker, "Focus issue: Light scattering by non-spherical particles," Opt. Express **8**, 288–289 (2001).
40. Y. Eremin and N. Orlov, "Modelling of light scattering by non-spherical particles based on discrete sources method," J. Quant. Spectrosc. Radiat. Transf. **60**, 451–462 (1998).
41. H. Raether, *Surface Plasmons* (Springer-Verlag, Berlin, 1988).
42. J. R. Sambles, G. W. Bradberry, and F. Yang, "Optical-excitation of surface-plasmons—an introduction," Contemp. Phys. **32**, 173–183 (1991).
43. E. A. Perkins and D. J. Squirrell, "Development of instrumentation to allow the detection of microorganisms using light scattering in combination with surface plasmon resonance," Biosens. Bioelectron. **14**, 853–859 (2000).